8180–8192 *Nucleic Acids Research, 2019, Vol. 47, No. 15* *Published online 31 May 2019*
doi: 10.1093/nar/gkz486

The glucocorticoid receptor DNA-binding domain recognizes RNA hairpin structures with high affinity

Nicholas V. Parsonnet, Nickolaus C. Lammer, Zachariah E. Holmes, Robert T. Batey* and Deborah S. Wuttke*

Department of Biochemistry, University of Colorado at Boulder, Campus Box 596, Boulder, CO 80309-0596, USA

Received March 13, 2019; Revised May 17, 2019; Editorial Decision May 20, 2019; Accepted May 21, 2019

ABSTRACT

The glucocorticoid receptor (GR) binds the noncoding RNA Gas5 via its DNA-binding domain (DBD) with functional implications in pro-apoptosis signaling. Here, we report a comprehensive *in vitro* binding study where we have determined that GR-DBD is a robust structure-specific RNA-binding domain. GR-DBD binds to a diverse range of RNA hairpin motifs, both synthetic and biologically derived, with apparent mid-nanomolar affinity while discriminating against uniform dsRNA. As opposed to dimeric recognition of dsDNA, GR-DBD binds to RNA as a monomer and confers high affinity primarily through electrostatic contacts. GR-DBD adopts a discrete RNA-bound state, as assessed by NMR, distinct from both free and DNA-bound. NMR and alanine mutagenesis suggest a heightened involvement of the C-terminal α-helix of the GR-DBD in RNA-binding. RNA competes for binding with dsDNA and occurs in a similar affinity range as dimer binding to the canonical DNA element. Given the prevalence of RNA hairpins within the transcriptome, our findings strongly suggest that many RNAs have potential to impact GR biology.

INTRODUCTION

The glucocorticoid receptor (GR) is a ubiquitously expressed DNA-binding transcription factor (TF) that directly regulates thousands of genes associated with stress response, inflammation, and apoptosis (1–5). GR is often dysregulated in disease and is the target of commonly prescribed synthetic glucocorticoids used to combat a range of disorders including rheumatoid arthritis, chronic obstructive pulmonary disease, and many cancer types, often as part of a combinatorial treatment (6–9). Transcriptional regulation by GR requires glucocorticoid binding in the cytoplasm, triggering translocation to the nucleus and interaction with the genome via the DNA-binding domain (DBD). Direct genomic binding is typically associated with transcriptional activation and DBD mutants show defects in glucocorticoid response (10,11). DNA-binding by the GR-DBD has been well-characterized; it is highly sequence-specific, directly recognizing invariant guanine nucleotides of two AGAACA half sites called the glucocorticoid response element (GRE), and binds as a dimer in head-to-head orientation with mid-nanomolar affinity (4,12–18).

In contrast, RNA recognition by GR is relatively poorly understood, although several reports detail GR binding to biological RNAs including tRNA, mRNA, and Gas5 long noncoding RNA (lncRNA) (19–22). The most intriguing and thoroughly investigated example is the functional interaction between GR-DBD and Gas5 (19,20). Gas5 is highly expressed upon growth arrest and stimulates cell death through several pro-apoptotic roles (23–29). Gas5 has been shown to negatively regulate miR-21, an anti-apoptotic microRNA upregulated in cancer, by acting as a microRNA sponge (30,31). Additionally, Gas5 has been shown to act as an RNA repressor of GR with pro-apoptotic consequence (19,20). Downregulation of Gas5 has anti-apoptotic effects in cell culture and is correlated with poor prognosis for prostate and breast cancers (20,24,27,28).

A GRE-like element within Gas5 RNA is proposed to repress GR by acting as a molecular decoy for the GR-DBD (19,20). This mechanism is of acute interest as RNA-binding activities of other DNA-binding proteins continue to be uncovered. For example, the DBDs of YY1, SMAD3, TFIIIA, NF-kB, and KpnI (restriction enzyme) bind RNA with varying levels of specificity that largely do not correlate with known DNA counterparts (32–43). Other transcription factors have been implicated by high-throughput RNA-binding proteomic studies, but the specificity and mechanisms involved are still unknown (44–46).

Here, we use the Gas5-GR interaction as a platform to probe the *in vitro* RNA-binding characteristics of GR-DBD to understand the mechanism and rules of RNA-DBD interaction. We find that GR-DBD binds to RNA hairpins in a structure-specific rather than sequence-specific manner. GR-DBD binds to RNA as a monomer and uses elec-

*To whom correspondence should be addressed. Tel: +1 303 492 4576; Email: Deborah.Wuttke@colorado.edu
Correspondence may also be addressed to Robert T. Batey. Email: Robert.Batey@colorado.edu

trostatic contacts to confer high affinity. NMR studies suggest that GR-DBD adopts a discrete RNA-bound state and implicates the involvement of the C-terminal α-helix, confirmed by protein mutagenesis. Contrary to previous reports, our results reveal that RNA-binding by GR-DBD is not limited to Gas5 RNA and broadly implicate structured RNAs in direct regulation of GR-mediated gene expression.

MATERIALS AND METHODS

Glucocorticoid receptor DNA-binding domain expression, purification, and activity

The human glucocorticoid receptor DNA-binding domain (residues 421–506) was expressed with a thrombin-cleavable N-terminal hexahistidine tag using a pET28a (EMD Biosciences) vector (generous gift from the Keith Yamamoto Lab, UCSF). Protein expression methods were adapted from established protocols (15). Starting with a single transformed colony of BL21(DE3) *Escherichia coli*, expression cultures were grown at 37°C (with 50 μg/ml kanamycin) using 2× YT rich media to an OD_{600} of 0.8–1.0 and cold shocked on ice for 20 min. Isopropyl β-D-thiogalactopyranoside was added to a final concentration of 0.3 mM to induce protein expression and cultures were grown for 4–5 h at 25°C. Cells were harvested by centrifugation (5000 RCF) and pellets stored at −20°C.

Cell pellets were thawed and resuspended in 50 ml lysis buffer (20 mM Tris pH 7.5, 1 M NaCl, 10 mM imidazole pH 7.5, 5% glycerol) per 1 l of cells with one EDTA-free protease inhibitor cocktail tablet (Roche). Cells were lysed using a Misonix Sonicator 3000 (110 W for 2 min total ON-time, pulse: 15 s ON/45 s OFF, $\frac{1}{2}$ inch tip) and the lysate cleared by centrifugation (15 000 RCF, 30 min). Cleared lysate was loaded onto lysis buffer-equilibrated Ni-NTA resin (GoldBio, 5 ml resin per 50 ml lysate) and rocked gently for 1 h at 4°C. The bead slurry was loaded onto a gravity flow column and washed twice with increasing concentrations of imidazole in lysis buffer (Wash1: 20 mM imidazole, Wash2: 30 mM imidazole), then eluted with 300 mM imidazole in lysis buffer. Bovine α-Thrombin (Haematologic Technologies Incorporated) was added (10 U/mg protein) to the eluate to remove the hexahistidine tag. The eluate solution was transferred to 6–8K MWCO dialysis tubing (Spectra/Por – Spectrum Labs) and dialyzed overnight at 4°C in 4 l of column buffer (20 mM Tris pH 7.5, 100 mM NaCl, 5% glycerol, 1 mM DTT).

Dialyzed eluate was filtered to 0.2 μm and concentrated using 5K MWCO spin concentrators (Vivaspin Turbo). The sample was again filtered to 0.2 microns and loaded onto a HiLoad 16/600 Superdex 75 column (GE Healthcare) and eluted as a monomer. Pooled fractions containing recombinant GR-DBD were assessed for purity, aliquoted, flash-frozen, and stored at −70°C. One liter of media typically yielded 2 mg of purified GR-DBD ($\varepsilon = 4470\ M^{-1}\ cm^{-1}$) (47).

GR-DBD preparations were assayed for activity by binding to dsDNA GRE consensus using electrophoretic mobility shift assays (48). dsDNA was held constant at 10 μM to 15 μM (1 nM fluorescently labeled) while GR-DBD was titrated. Gels were imaged using a Typhoon Imager (GE Healthcare), quantified by ImageQuant, and activity calculated assuming 2:1 protein to DNA stoichiometry. Activity corrections typically ranged from 0.7 to 1.3-fold. N-terminally His-tagged GR-DBD was used for some binding experiments included in the supplemental data. Purification was identical to above, with omission of thrombin prior to dialysis. We found that the His-tagged version of GR-DBD consistently bound RNA 6.4-fold tighter, thus affinities determined with the His-tagged protein were adjusted for this difference to allow comparison of relative binding affinities. They are reported as $K_{D,adj}$ (equal to $6.4*K_{D,app}$) where relevant.

Protein preparation for alanine mutants

GR-DBD mutants were created by site-directed mutagenesis by QuikChange protocols (Stratagene) and sequence-verified. Purifications were performed using an abbreviated version of the protocol above and are identical up to the dialysis step. After dialysis and thrombin cleavage, dialyzed eluate was filtered to 0.2 microns and incubated with 0.5 ml buffer-equilibrated Ni-NTA beads for 1 h at 4°C, then eluted as flow-through and concentrated using 5K MWCO spin concentrators (Vivaspin Turbo). Protein concentrations were determined by spectrophotometry (A_{280}) and independently validated using standardized SDS-PAGE quantification. Affinity is reported as fold change relative to wild type GR-DBD prepared for this assay.

Oligonucleotide preparation

All sequences used for binding experiments are listed in Supplemental Table S1. DNA oligonucleotides were ordered from Integrated DNA Technologies (IDT) with standard desalting. For fluorescently labeled constructs used in anisotropy measurements, the sense strand was synthesized with fluorescein conjugated to the 5′-end. The labeled and unlabeled complementary strands were annealed by slow cooling (thermocycler: 95°C, then −0.1°C/s to 25°C) at 1 μM in annealing buffer (20 mM Tris pH 7.5, 50 mM NaCl).

RNA oligonucleotides were prepared by *in vitro* transcription using T7 RNA polymerase and dsDNA templates created from IDT-synthesized oligonucleotides (49). After transcription, RNAs were purified by denaturing polyacrylamide gel electrophoresis (1× TBE/8 M urea) (50). Purified RNA oligonucleotides were 3′-end labeled with fluorescein 5-thiosemicarbazide (FTSC) using protocols adapted from published methods (51). 350 pmol RNA was treated with sodium periodate (0.02 M) for 20 min at room temperature, potassium chloride was added to 25 mM, incubated on ice 10 min and pelleted by centrifugation (14000 RCF, 20 min). Supernatant was transferred to a clean tube, ethanol precipitated (with 20 μg glycogen), and washed with 70% ethanol. The pellet was dried, then resuspended in labeling solution (1.5 mM FTSC, 100 mM sodium acetate pH 5.2), incubated at 37°C for 1 h, ethanol precipitated, and washed with 100 μl of 70% ethanol 5 times. The RNA pellet was dried, then resuspended in 30 μl of annealing buffer, passed through a G-25 spin column, and stored at −20°C. Concentration was determined by A_{260} and total RNA yield was typically 10–

50% with ∼20% labeling efficiency. Purity of the final sample was assessed by 10–15% denaturing PAGE and imaged by fluorescence.

DNA and RNA samples were prepared for binding assays by annealing (dsDNA or dsRNA constructs) or fast refolding (RNA). For annealing, the labeled and unlabeled strands were diluted to 1 μM in folding buffer (20 mM Tris pH 7.5, 10 mM NaCl). RNAs were refolded at 1 μM by snap-cooling (95°C for 1 min, ice for >5 min).

High-resolution thermal melts were used to verify RNA hairpin and duplex formation. Nucleic acid samples were prepared at 3 μM in melting buffer (1× SybrGreen I, 10 mM potassium phosphate, 100 mM NaCl). Thermal melts were performed from 20°C to 95°C at 1°C increments (Applied Biosystems StepOnePlus). Melting temperatures were determined by first derivative analysis. To predict the structure of Gas5 RNA *in vivo,* we used publicly available ic-SHAPE data (GEO: GSE74353) as a restraint for RNA folding (RNAprobing algorithm, Vienna Suite) (52,53).

Fluorescence anisotropy assays

All binding experiments were performed at least in triplicate on different days with independent dilutions and remained consistent across protein preparations. Apparent affinities were measured at equilibrium by fluorescence anisotropy (FA) methods adapted from published protocols (54). Error is reported as standard error from the mean. Reactions were prepared in binding buffer (20 mM Tris pH 7.5, 100 mM NaCl, 5% glycerol, 0.01% IGEPAL). Protein titrations (typical titration range: 10 μM to 0.02 nM) against labeled nucleic acids (typically 1–5 nM) were performed in 384-well plates (24 reactions per titration, 20 μl reactions) and allowed to equilibrate for 1 h at room temperature. Polarized fluorescence intensity values were collected with the CLARIOstar High Performance Plate Reader (BMG) and used to calculate anisotropy. Titrations were fit to the single-site binding equation, $A = O + (S*P)/(P + K_D)$, using KaleidaGraph, where P is the concentration of GR-DBD, A is anisotropy, O is baseline offset for free oligonucleotide, and S is the value for fully bound oligonucleotide at saturation. Our calculations operate under the assumption that protein is in sufficient excess over labeled ligand to avoid an exact treatment that requires accurate quantitation of all components of the reaction. This assumption has been shown to be valid in the regime where the ligand is in 5-fold excess; here all reported $K_{D,app}$ values are at minimum 10-fold above the concentration of respective ligand and thus well within experimentally determined limits (55). Typical anisotropy values for O (free) and S (bound) were 0.06 and 0.20 for DNA, and 0.06 and 0.16 for RNA, respectively. Hill coefficients (n) were calculated using the simplified Hill equation, $A = O + (S*P^n)/(P^n + K_D)$.

Salt dependence experiments were adapted from published studies (56). Affinity measurements were performed with salt binding buffer (20 mM Tris pH 7.5, 0.01% IGEPAL, 5% glycerol, with NaCl concentrations of 75, 100, 125, 150 and 175 mM). Double log plots were fit to a linear equation, $\log(K_a) = \log(K_{a,nel}) - N*\log[NaCl]$, where N (slope) is $Z*0.7$, Z is the number of electrostatic contacts, and $\log(K_{a,nel})$ is the non-electrostatic component (56). This analysis assumes an infinite line charge where individual segments are effectively screened from each other (57,58) which may not accurately predict the behavior of short oligonucleotides, possibly causing an overestimation of the energetic contribution of the non-electrostatic component.

NMR analysis

NMR samples were prepared at 1.2:1 nucleic acid to protein ratio in NMR buffer (20 mM sodium phosphate pH 6.7, 100 mM NaCl, 1 mM DTT) (17). Protein and nucleic acid were buffer exchanged separately then mixed at a volumetric ratio of 1:1 and concentrated by 3K MWCO spin concentrator (Millipore) and D_2O added to 10%. The sample was transferred to a Shigemi NMR sample tube and equilibrated to room temperature. The typical concentration of GR-DBD was 150 μM.

NMR experiments were collected at 30°C on an Agilent 600 MHz NMR spectrometer equipped with an HCN triple resonance warm probe using TROSY-HSQC Biopack pulse sequences (nt = 128, ni = 256) with minor modifications. Data were processed using standard processing parameters with NMRPipe and analyzed with CcpnmrAnalysis. Peak assignments were transferred to our spectra from published reports and by chemical shift difference minimization (17). Ambiguous peaks were left unassigned. Chemical shift difference (CSD) was calculated as average Euclidean distance by $(0.5(\Delta\delta_H^2 + 0.17*\Delta\delta_N^2))^{1/2}$ and a threshold of 0.04 used to identify significantly shifted residues (59). Tabulated chemical shift assignments and CSD values are listed in Supplemental Table S2.

RESULTS

GR-DBD binds to a Gas5 RNA hairpin with comparable affinity to consensus DNA

Previous *in vitro* binding studies demonstrated a high affinity interaction between GR-DBD and Gas5 RNA (19,20). To further investigate the RNA-binding properties of GR-DBD, we first benchmarked our samples and methods against published binding data using a fluorescence anisotropy (FA) assay. The consensus DNA glucocorticoid response element (GRE) is comprised of two half-sites (AGAACA) separated by a three base-pair spacer (13,15,60,61). We found that the (+)GRE consensus sequence (referred to here as DNA-GRE) bound GR-DBD with a $K_{D,app}$ of 67 ± 7 nM (Figure 1A and D), in good agreement with the published value of 73 ± 7 nM (16). Published data shows that the Gas5 hairpin effectively competes with DNA for binding to GR-DBD exhibiting a $K_{i,app}$ of 125 nM (20). We used established methods for 3′-end fluorescein labeling of RNA to probe RNA-binding directly using fluorescence anisotropy (51). For the previously reported Gas5 hairpin (single-stranded regions trimmed, 43-nucleotide construct), we observe a $K_{D,app}$ of 67 ± 9 nM (Figure 1B and D), in good agreement with the published $K_{i,app}$, reaffirming the observation that RNA binds in a similar affinity regime to DNA-binding by GR-DBD. Additionally, we independently confirmed that Gas5 RNA effectively competes for binding with the consensus DNA construct (Supplemental Figure S1).

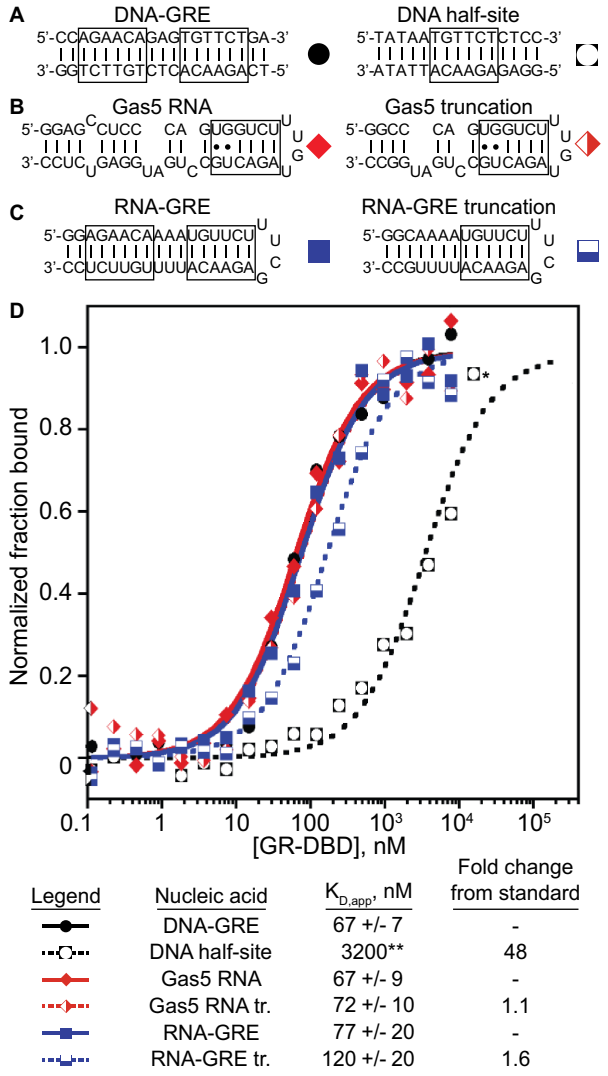

Figure 1. GR-DBD binds to DNA and RNA with different stoichiometries. DNA and RNA constructs used to determine apparent dissociation constants ($K_{D,app}$ values are reported with standard error from the mean) for wild type sequences (left column) and half-site truncations (right column) for (**A**) DNA-GRE, (**B**) Gas5 RNA hairpin and (**C**) RNA-GRE. GRE half-sites or equivalent are boxed. Gas5 contains only one putative GRE-like half-site and so was length-matched to other truncations. (**D**) Representative, normalized binding curves for wild type sequences (solid lines) and half-site truncations (dashed lines) for DNA-GRE (black circles, $n = 9$), DNA half-site (open black circles, $n = 4$), Gas5 RNA (red diamonds, $n = 13$), Gas5 truncation (open red diamonds, $n = 4$), RNA-GRE (blue squares, $n = 4$), and RNA-GRE truncation (open blue squares, $n = 4$). DNA half-site truncation binds too weakly to measure accurately, so a lower limit was estimated by extrapolating the highest measured value, marked by (*), as the fully-bound state – error is not reported and is indicated by **.

We assessed cooperative binding to the DNA-GRE and the Gas5 hairpin by fitting our binding data to the Hill equation for the wild type GR-DBD construct. The Hill coefficient for DNA is 1.3 ± 0.1, consistent with the value of 1.4 reported previously (16), and for RNA is 0.93 ± 0.04, suggesting that while GR-DBD binds with mildly positive cooperativity to DNA, cooperative binding to RNA is not observed.

GR-DBD dimerizes on DNA but not RNA

It is well established that GR-DBD binds to consensus DNA elements as a dimer in head-to-head orientation with positive cooperativity (13,15). In a fundamental departure from this canonical mode of DNA binding, prior NMR data suggests that GR-DBD does not dimerize upon binding to a 33-nucleotide Gas5 RNA hairpin (20). Given that DNA and RNA show nearly identical affinities in our assay, we were intrigued by this apparent difference in dimerization behavior. To directly investigate the relative effects of dimerization on DNA and RNA affinity, we characterized nucleic acid binding using a dimerization mutant of GR-DBD. Alanine 458 resides in the dimerization loop and disruption is reported to decouple binding between the two half-sites (17). GR-DBD with a mutation at this site, A458T, showed ∼3-fold weaker binding to DNA-GRE (220 ± 50 nM) but maintained full affinity for the Gas5 hairpin construct (70 ± 10 nM) supporting the notion that RNA-binding is dimerization-independent.

Next, we directly measured the affinity of monomeric GR-DBD for DNA and RNA by truncation of the oligonucleotide to enforce a 1:1 stoichiometry. The DNA-GRE was shortened such that only one half-site remained and Gas5 wild type hairpin was truncated to a similar length (Figure 1B). GR-DBD binding to these half-site deletions showed over 20-fold weaker affinity for DNA (lower limit of 3200 nM* estimated by assuming that the maximum anisotropy value represents the fully bound state, also see Figure 1 legend) while a similar truncation for Gas5 has little effect (70 ± 20 nM). Weak binding to the DNA half-site, as opposed to maintenance for the Gas5 truncation, demonstrates a fundamental difference in stoichiometry.

RNA-binding by the GR-DBD is driven by electrostatic interactions

The difference in GR-DBD stoichiometry suggests an underlying disparity between DNA- and RNA-binding modes. We hypothesized that the RNA-GR-DBD complex would utilize additional electrostatic contacts to achieve high affinity at 1:1 stoichiometry. To empirically determine the contribution of electrostatic interactions to affinity, we measured the salt dependence of binding for DNA-GRE and Gas5 RNA (Figure 2A). As expected, both binding events are highly salt dependent, with thermodynamic analysis revealing utilization of 6.3 ± 0.1 and 8.1 ± 0.3 electrostatic contacts for DNA-GRE and Gas5 hairpin RNA, respectively (Figure 2B). While these values appear similar, they show a marked difference once corrected for binding stoichiometry. As GR-DBD binding to DNA-GRE occurs at 2:1 protein to DNA, there are an average of 3.2 electrostatic contacts per GR-DBD monomer, in good agreement with available crystal structures of GR-DBD bound as a dimer to consensus DNA (13,15). Salt-dependent binding to the DNA half-site shows 4.1 ± 0.1 electrostatic contacts, supporting this observation (Figure 2A and B). When compared to RNA, both DNAs tested employ half of the total electrostatic contacts per monomer.

To assess whether the enforced 1:1 DNA-binding represents a similar DNA-bound conformation as the dimer, we collected the ^{1}H–^{15}N HSQC NMR spectrum for GR-DBD

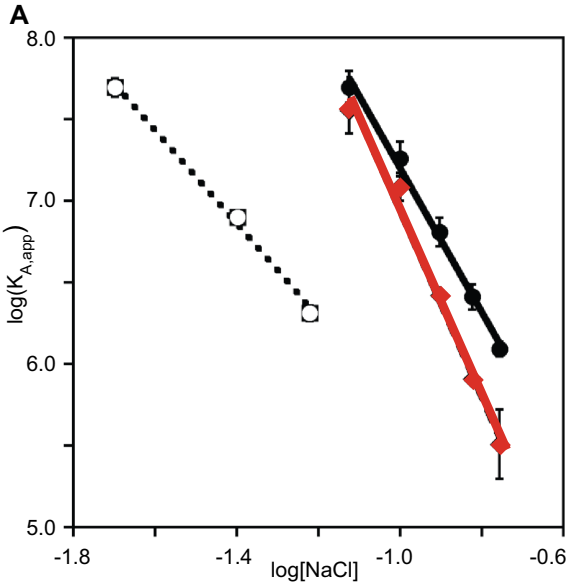

B

	DNA-GRE	DNA half-site	Gas5 RNA
Slope	4.4	2.9	5.7
y-intercept	2.8	2.8	1.2
Contacts	6.3 +/- 0.1	4.1 +/- 0.1	8.1 +/- 0.3
$\Delta G_{electrostatic}$	-25 kJ/mol	-17 kJ/mol	-33 kJ/mol
$\Delta G_{non\text{-}electro}$	-16 kJ/mol	-16 kJ/mol	-7 kJ/mol

Figure 2. Salt dependence reveals differences in electrostatic contributions of binding of GR-DBD to DNA and RNA. (**A**) Double-log plot of GR-DBD binding constants versus concentration of sodium chloride for DNA-GRE (black line, closed circles), DNA half-site (dashed black line, open circles), and Gas5 RNA hairpin (red line, diamonds). Curves were fit to the linear salt-dependence equation, as described (56,98). Slope and y-intercept values are displayed in (B). Experiments were performed in triplicate and reported with standard error from the mean. R^2 values are 0.99, 0.99 and 0.99, respectively. (**B**) Slope, y-intercept, # of electrostatic contacts, and energetic contributions of electrostatic and non-electrostatic components calculated at 100 mM sodium chloride.

bound to the single DNA half-site (Supplemental Figure S2). Chemical shifts agree well with spectra previously observed for the dimer (17), with the primary differences manifesting in the dimerization loop, suggesting the enforced monomer binds its half site in a similar conformation as the structurally characterized dimer, albeit with greatly reduced affinity. Thus, the recognition of nucleic acid on a per-protein basis involves significantly more electrostatic interactions to RNA than to DNA, supporting a distinct mode of recognition.

RNA-binding is not mediated by GRE-derived sequence-specific contacts

DNA-binding by GR-DBD occurs through base-specific recognition of the invariant guanine nucleotides within palindromic half-sites (consensus half-site AGAACA) of the GRE (13,15,60,61). Gas5 RNA contains a segment resembling this DNA half-site sequence (Figure 1A and B, compare boxed elements – 66% identity) and is proposed to act as a GRE-mimic through similar presentation of

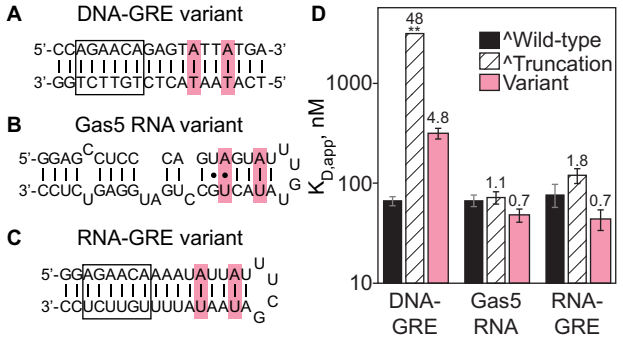

Figure 3. DNA and RNA do not show similar sequence specificity. Wild type sequences for (**A**) DNA-GRE, (**B**) Gas5 RNA hairpin and (**C**) RNA-GRE were changed to ablate a single half-site at base-pairs highlighted (pink). (**D**) $K_{D,app}$ values of wild type sequences (black), half-site truncations (striped), and half-site variants (pink). Fold change from standard indicated above bar. DNA-GRE, Gas5 RNA and RNA-GRE variant sequences bind with apparent dissociation constants of 320 ± 40 nM ($n = 5$), 48 ± 7 nM ($n = 5$) and 44 ± 10 nM ($n = 4$), respectively. Half-site sequences are boxed. (^) Data for wild type and truncation constructs located in Figure 1D. All data tabulated in Supplemental Table S3.

the guanine nucleotides via a widened RNA major groove (20). We sought to investigate the role of these guanine nucleotides in binding to GR-DBD for both DNA and RNA, which show thermodynamically equivalent binding above. Using the direct binding FA assay, we measured the affinity of guanine variants for each nucleic acid. As expected, changing G–C pairs to A–T pairs in the DNA consensus half-site weakens the apparent affinity nearly 5-fold ($K_{D,app}$ of 320 ± 40 nM) (Figure 3A and D). In contrast, similar variation of one or both of the equivalent guanines in Gas5 shows no effect ($K_{D,app}$ of 48 ± 7 nM) (Figure 3B and D, Gas5 G549A in Supplemental Table S3). This unexpected result demonstrates that the GRE-like sequence element within the Gas5 hairpin is not specifically recognized and in fact is not required for high affinity binding.

Given the minimal sequence preference observed for the Gas5 hairpin binding, we investigated the sequence-structure features driving binding affinity. To test this, we rendered the DNA consensus sequence into a uniform RNA hairpin, termed the RNA-GRE, devoid of bulges, internal loops, and tandem G–U pairs (Figure 1C). The RNA-GRE binds to GR-DBD with similar affinity to consensus DNA and Gas5 hairpin constructs (77 ± 10 nM) (Figure 1D). Like the Gas5 RNA, the RNA-GRE maintains tight affinity even when the consensus half-site is ablated (44 ± 10 nM) or truncated (120 ± 20 nM) (Figures 1C and D, 3C and D). These results suggest that GR-DBD has a more broad and flexible RNA-binding capacity than anticipated, in contrast to other reports (19,20).

High affinity RNA-binding by GR-DBD requires a hairpin RNA structure

The maintenance of high affinity binding in the absence of stem features, in addition to the lack of sequence specificity observed for the Gas5 hairpin, pointed to the tetraloop (4-base loop) as the commonly recognized feature. To test whether the hairpin is required for high affinity binding, we

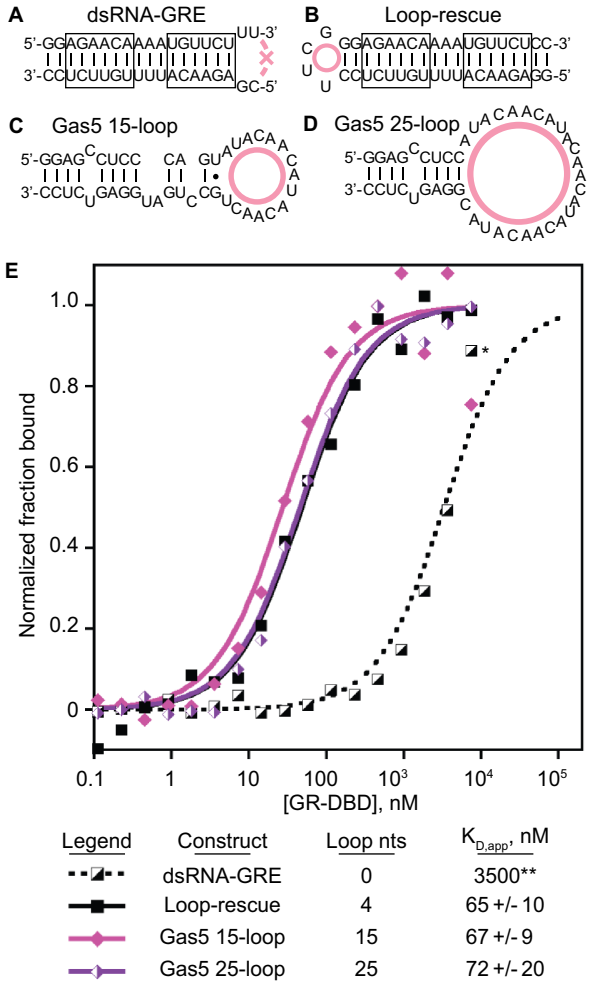

Figure 4. RNA loop is required for binding. Nucleic acid construct schematics for (**A**) dsRNA-GRE ($n = 7$), (**B**) loop-rescue for dsRNA-GRE ($n = 3$), (**C**) Gas5 15-nucleotide loop ($n = 4$) and (**D**) Gas5 25-nucleotide loop ($n = 4$), with pink circles indicating incorporated variations. Loop expansion variations of Gas5 (C and D) were made by replacing the tetraloop and adjacent nucleotides with repeats of a single-stranded RNA linker (AUACAAC) (67). (**E**) Binding curves and $K_{D,app}$ values, noting the number of loop nucleotides predicted upon folding (99). Error reported as standard error from the mean. dsRNA-GRE binds too weakly to measure accurately, so a lower limit was estimated by extrapolating the highest measured value, marked by (*), as the fully-bound state – error is not reported and is indicated by **.

created a double-stranded RNA (dsRNA) construct containing the same sequence as the RNA-GRE with the loop ablated (Figure 4A). Unexpectedly, we observe a dramatic decrease in binding affinity. Due to this weak binding, it is difficult to measure the dissociation constant with high certainty; estimating the a $K_{D,app}$ value by assuming that the maximum anisotropy value represents the fully bound state reveals a lower limit of 3500 nM for dsRNA-GRE binding, representing at least an 30-fold reduction in affinity. We used melting temperature and gel shift analysis to confirm that the dsRNA construct annealed as expected and remained double-stranded over the course of the experiment (Supplementary Figure S3). Similarly, a DNA/RNA hybrid duplex of the same length and sequence showed binding too weak to measure accurately (Supplemental Table S3), suggesting a solely A-form helix does not support binding.

These results suggest that a hairpin, as opposed to just dsRNA, is required for high affinity binding to GR-DBD. To further test this hypothesis, we designed a rescue construct via circular permutation of the RNA-GRE by adding back a tetraloop to the opposing end of the duplex. This rescued hairpin binds with 65 ± 10 nM affinity (Figure 4 B) suggesting that the hairpin structure is sufficient to confer high affinity regardless of orientation and sequence context.

To test the effect of terminal loop for the Gas5 wild type hairpin, we similarly rendered this stem as a dsRNA construct (dsRNA-Gas5). To create constructs with tractable melting temperatures for *in vitro* binding, we created two separate constructs: (i) adding a 3-base-pair GC-clamp (opposite the former loop), termed 'dsRNA-Gas5-GC' and (ii) eliminating bulges and internal loops, termed 'Full-Repair'. Annealing was confirmed by direct melting temperature measurement as above (dsRNA-Gas5-GC: predicted 68.6°C, measured 68°C; Full-Repair: predicted 82°C, measured 78°C). We attempted to measure the affinity of these dsRNA constructs for GR-DBD, but similarly were not able to determine the affinity due to no observed change in anisotropy over the course of the titration up to protein concentrations of 10 μM (Supplemental Table S3). These results affirm that wild type Gas5 hairpin requires the loop for high affinity.

Given that the dsRNA-GRE construct removes the longest contiguous single-stranded segment of the RNA-GRE construct (the loop), we tested whether the degree of single-stranded character correlates with affinity. Using the dsRNA-GRE as a platform, we designed a set of constructs that maintain the double-stranded region while sequentially increasing the single-stranded overhang up to 18 nucleotides (Supplemental Figure S4). For all RNAs tested, we observe no detectable binding over the course of the titration (Supplemental Table S3), indicating that high affinity binding is not conferred by the simple coincidence of single- and double-stranded elements.

GR-DBD binds well to several biological RNA hairpins

GR-DBD is proposed to specifically recognize the Gas5 RNA via a GRE-mimic sequence–a discrete hairpin spanning nucleotides 538-576 (19,20). Gas5 is more than 600 nucleotides in length and predicted to be highly structured (62–64). Based on our results showing that GR-DBD binds a range of hairpin structures, we reexamined the ability of GR-DBD to bind other Gas5-derived hairpins. An additional three predicted Gas5-derived hairpins with no discernable sequence similarity to the Gas5 GRE-mimic sequence were tested for binding (all length-matched 59-nucleotide constructs, Supplemental Figure S4). All four Gas5-derived hairpin constructs bind with similar high affinity with $K_{D,app}$ values of 15 ± 3, 31 ± 10, 60 ± 20 and 17 ± 2 nM, respectively (Supplementary Table S3). This demonstrates that GR-DBD is not able to discriminate between Gas5 hairpins in an isolated context.

Given the high affinity observed across all Gas5-derived hairpins tested, we hypothesized that GR-DBD may interact with unrelated hairpins with similar affinity. We ob-

tained RNA hairpin constructs derived from the human lncRNAs *ES2* and *Xist* and observe 130 ± 40 and 66 ± 10 nM affinity for GR-DBD, respectively, suggesting a modest level of differential binding, but overall robust binding to unrelated hairpin structures (Supplemental Figure S4, Supplemental Table S3) (65,66).

High affinity RNA-binding by GR-DBD is supported by a range of hairpin structures

RNA hairpin structures are required for high-affinity recognition by GR-DBD, but the specific elements present in this context may also contribute to binding. To identify contributing elements, we modified duplex and loop length separately to systematically eliminate putative features (e.g., internal loops, bulges, G–U wobble-pairs) by replacement with single-stranded sequences (CA-repeats or single-stranded RNA linker, AUACAAC, from the unrelated *env8* hydroxycobalamin riboswitch (67)) while controlling for length. To test duplex length, Gas5 hairpin RNA was essentially 'unzipped' from the base of the stem, moving towards the loop, to give paired regions of 13, 9, 7 and 4 bp, yielding $K_{D,adj}$ values (compared to Gas5 wild type hairpin, see methods) of 66 ± 20, 72 ± 10, 51 ± 20 and 120 ± 30 nM, respectively (Supplemental Figure S4, Supplemental Table S3). This series demonstrates that a 4-base-pair stem loop is sufficient for binding and suggests that the sequence of the Gas5 stem is not a determining factor.

We next investigated how sequence and length of the loop of the hairpin dictate affinity by creating a series of RNA loop expansion and substitution variants and measured affinity for GR-DBD (Figure 4C and D, Supplemental Figure S4). Essentially, Gas5 hairpin RNA was opened from the loop down, while maintaining construct length. We measured the affinity for predicted loop sequences of 15-nt and 25-nt which bind with 32 ± 5, and 67 ± 9 nM affinity, respectively (Figure 4C–E). As all loop expansion variants maintain affinity equal to or tighter than the wild type Gas5 hairpin, we determined that loop length is not a determining factor for binding.

All RNA hairpins engage GR-DBD equivalently as assessed by NMR

The high binding affinities exhibited by the GR-DBD across a wide range of RNA hairpins suggests that GR-DBD is capable of broad RNA recognition. To determine the scope of GR-DBD surfaces used to engage RNA, we used ^{1}H–^{15}N HSQC NMR experiments to probe the GR-DBD in several RNA-bound complexes. The reported ^{1}H–^{15}N HSQC spectrum for GR-DBD bound to a 33-nucleotide derivative of the Gas5 RNA hairpin finds notable chemical shift changes in the reading helix (α-helix 1) of the DBD, consistent with competitive binding and suggesting a similar interface for DNA and RNA (20). To compare these data with our 43-nucleotide Gas5 RNA hairpin construct, we collected ^{1}H–^{15}N HSQC spectra for GR-DBD in the free and Gas5 RNA-bound state and transferred resonance assignments from published free and DNA-bound spectra using chemical shift difference (CSD) minimization (90% and 88% of cross peaks could be assigned for free and Gas5 RNA hairpin-bound, respectively) (Figure 5A) (17). The 43-nucleotide and 33-nucleotide derivatives of the Gas5 RNA hairpin exhibit nearly identical spectra with the exception that we observed less peak broadening and were able to make additional assignments, perhaps due to the reduced pH of the complex samples used in our NMR experiments. The RNA-bound GR-DBD exhibits smaller magnitude CSD values than for DNA-bound, as seen previously (17,20).

The similar affinities observed for GR-DBD binding RNA-GRE and Gas5 RNA hairpin constructs *in vitro* motivated comparison of bound conformations by NMR. The RNA-GRE contains a uniform stem (i.e., no predicted internal loops, bulges or wobble-pairs) yet maintains high affinity binding by the presence of the stem loop. An overlay of the ^{1}H–^{15}N HSQC spectra for GR-DBD bound to Gas5 RNA and RNA-GRE complexes reveals striking similarities, suggesting that these RNAs bind via the same interface and binding mode (Figure 5B and C). GR-DBD complex with dsRNA-GRE, which does not contain a terminal loop, again produced a similar spectrum despite significantly weaker affinity (Figure 5B and C). Direct comparison of the GR-DBD chemical shifts across all RNA-bound spectra indicates highly similar protein bound states that are distinct from both free and DNA-bound protein, suggesting a discrete and conserved RNA-bound state.

Comparative NMR chemical shift mapping and protein mutagenesis support overlapping yet distinct binding modes for DNA and RNA engagement

Comparison of spectra for GR-DBD bound to DNA half-site and Gas5 RNA was used to identify differentially affected residues that could point to the origins of the observed differential affinities (Figure 5C and D, Supplemental Table S2). The surface maps of the DNA and RNA interfaces for GR-DBD are distinct yet partially overlapping (Supplemental Figure S5). Differential chemical shift changes were noted in α-helices 1 and 2, as follows, and predictions were tested by site-directed mutagenesis. K442 and K446 (α-helix 1) show significant CSD values for DNA-bound, but not RNA-bound states (Figure 5A and B, Supplemental Table S2), suggesting this 'reading' helix contributes disproportionately to DNA binding. Indeed, the α-helix 1 double-mutant (K442A/K446A) shows 20-fold weaker DNA affinity (1300 ± 300 nM) and 4-fold weaker RNA affinity (260 ± 20 nM); the 5-fold difference suggests that α-helix 1 is primarily used for DNA recognition. α-helix 2 makes both DNA–protein and protein–protein contacts and CSD values for K467 and R470 are emphasized in the RNA-bound state. The α-helix 2 mutant (K467A/R470A) shows dramatically weakened binding to both nucleic acid constructs (too weak to measure, >2000 nM), indicating critical involvement at both interfaces. These results suggest that while α-helix 1 is involved to some extent in both DNA and RNA interfaces it contributes most to DNA-binding; in contrast α-helix 2 is required for both high affinity interactions.

Alanine scanning implicates α-helix 4 in recognition of RNA

The salt dependence study suggests that electrostatic interactions play an even greater role in RNA binding than DNA

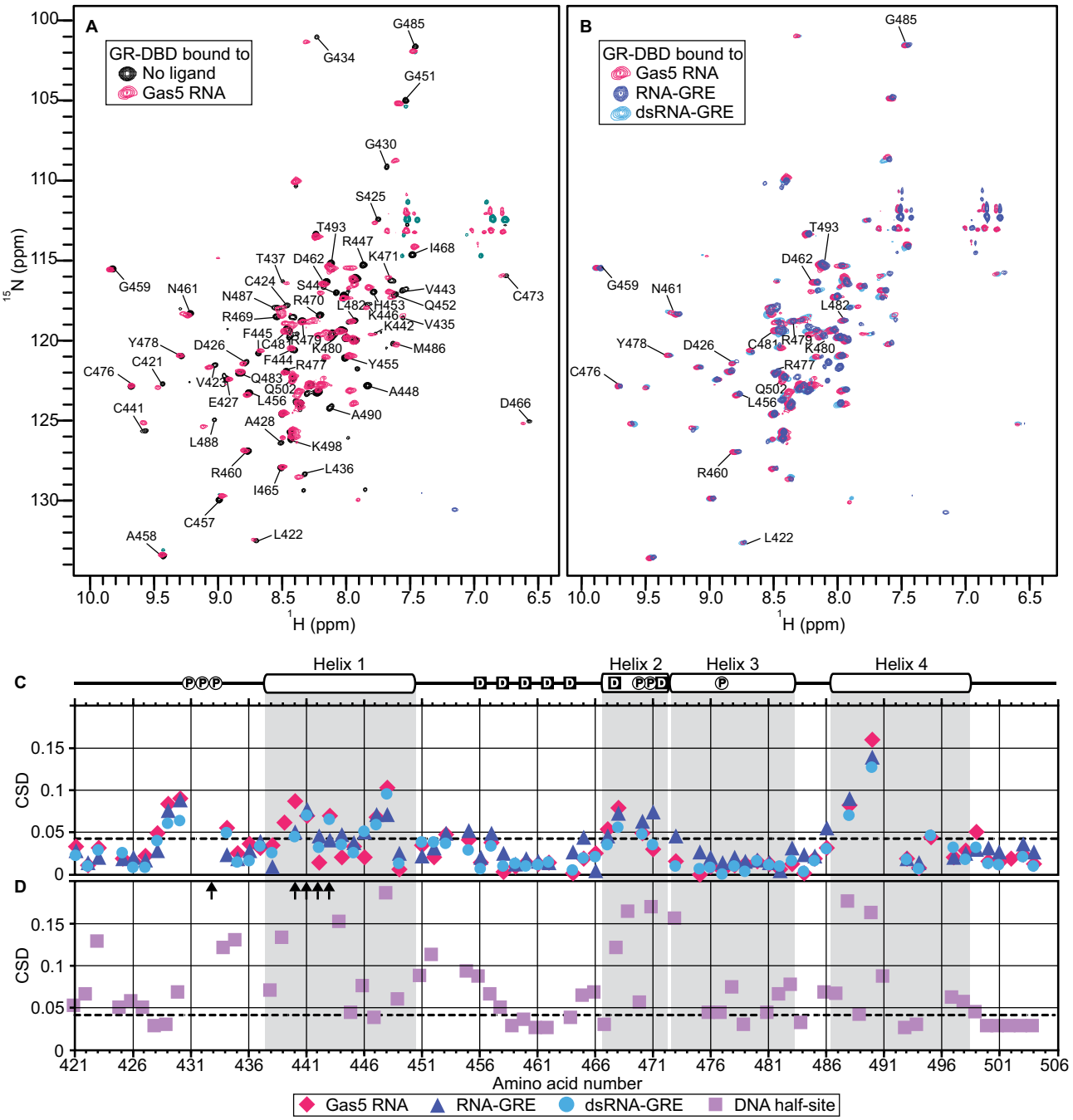

Figure 5. Chemical shift difference maps for DNA and RNA. (**A**) ^{1}H–^{15}N HSQC spectra for free (black) and Gas5 RNA-bound (magenta), assigned free peaks are labeled. (**B**) Overlay of Gas5 RNA-bound (magenta) with RNA-GRE (dark blue) and dsRNA-GRE (light blue). Peaks with CSD values less than 0.02 for all three RNAs are labeled, indicating minimal change from free. (C and D) Overlay of CSD values for (**C**) all RNA-bound spectra: Gas5 (magenta diamonds), RNA-GRE (dark blue triangles), and dsRNA-GRE (light blue circles); and (**D**) half-site DNA-bound spectrum. Horizontal dotted line represents CSD value of 0.04. Upwards arrows indicate value off scale. Protein features are annotated above plots: α-helices (white ovals, highlighted as gray boxes below), known DNA phosphate contacts (white circles), and dimer contacts (black squares) (13). For table of chemical shift differences see Supplemental Table S2.

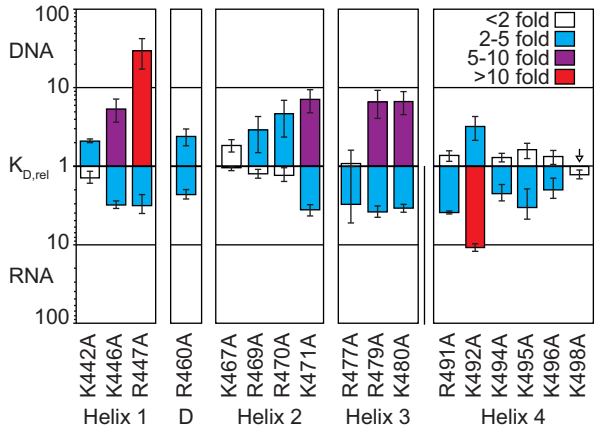

Figure 6. Role of electrostatic residues in DNA- and RNA-binding. Alanine scan of arginine and lysine residues (17 total) of the GR-DBD. Magnitude of mutant $K_{D,rel}$ ($K_{D,mut} \div K_{D,WT}$) for binding to DNA (upward) and RNA (downwards) by alanine mutants, as indicated. Boxes separate distinct features of the GR-DBD: α-helix 1, dimer-loop (D) and α-helices 2–4. Mutant $K_{D,rel}$ values are colored by fold change from wild type DBD: <2 (white), 2–5 (blue), 5–10 (purple), >10 (red). All experiments were performed at least in triplicate with error reported as standard error from the mean.

binding, suggesting there could be positively charged amino acids that differentially participate in nucleic acid recognition. To determine if mutagenesis of a charged site could confer separation-of-function, we performed a comprehensive alanine scan of the 17 arginine and lysine residues of the GR-DBD and measured the affinities of this panel of mutants for DNA-GRE and Gas5 RNA (Figure 6, Supplemental Table S4). While mutation of some charged sites had negligible impact on binding, most had an impact on nucleic acid binding, with differential effects observed on DNA versus RNA binding. Alanine substitutions in the reading helix (α-helix 1) show major defects in DNA-binding with up to 30-fold weaker affinity (R447A), as expected, while RNA-binding remains relatively unaffected by these mutations. Alanine substitutions in α-helices 2 and 3 show effects on both ligands, with larger effects on DNA than RNA (K471A, R479A, K480A). Conversely, α-helix 4, which is observed as either ordered or disordered in crystal structures of GR-DBD (13,15,16,68), shows largely RNA-specific defects. K492A of α-helix 4 displays the largest observed decrease in RNA affinity with more than 10-fold weaker binding. This suggests a dominant electrostatic role of helix 4 at the RNA interface.

DISCUSSION

We have determined that GR-DBD is a robust structure-specific RNA-binding domain that binds to a diverse range of RNA hairpin motifs—both synthetic and biologically derived—with nanomolar (10^{-8} to 10^{-7} M) affinities. This is consistent with observations that GR binds cellular RNAs, including tRNA, mRNA and Gas5 lncRNA (19–22,69). However, these findings are distinct from reports that describe a dsDNA GRE-like element in Gas5 RNA as required for binding to GR-DBD (20). We were unable to recapitulate this sequence-dependent binding defect, perhaps because the Gas5-derived duplex used for prior *in vitro* specificity studies lacks an RNA terminal loop and binds with relatively weak 800 nM affinity (20). Instead, we observe that variants of GRE-like elements in RNA do not show significant binding defects, supporting a structure-specific rather than sequence-specific binding mode. Most importantly, our data do not support a sequence-specific DNA mimicry model. Other factors may contribute to specificity observed *in vivo,* including RNA tertiary structure, additional RNA-binding proteins, and RNA abundance and localization.

Instead of binding RNAs that serve as mimics of GRE dsDNA, we have determined that GR-DBD requires an RNA hairpin for high affinity binding. There are several structural constraints to contemplate when considering how the GR-DBD interacts with hairpin RNAs. Canonical RNA structures adopt A-form geometry characterized by a deep, narrow major groove typically incompatible with binding by structured protein elements. However, loop- or bulge-proximal major grooves of RNAs are often wider than canonical A-form helix, allowing structured protein elements to bind. Known examples of this type of recognition include phage ϕ21-BoxB RNA and HIV-1 Rev-RRE RNA, where α-helical protein structures fit in RNA major grooves near loops or bulges similar in width to the B-form DNA structure recognized by GR-DBD (13,70–73). Thus, the RNA stem loop motifs bound by GR-DBD may offer accessible conformations for high affinity accommodation of α-helical elements mediated by the junction of the helix and loop that optimizes the shape of the helix for recognition.

Even though the binding of RNA and DNA by GR-DBD is competitive, the details of the binding interactions differ suggesting distinct binding modes of the protein are employed for DNA versus RNA recognition. Specifically, the reading helix of GR-DBD that is key for sequence-specific DNA recognition is less important for RNA-binding. In contrast, α-helix 4 appears to be specific for interaction with RNA. Relatively little is known about the role of this helix in binding dsDNA. The helix appears in two crystal structures of the GR-DBD, one free and one DNA-bound, and may directly contact the minor groove of DNA (15,68). However, most crystals lack density for this region suggesting a flexible and disordered element (13,15,16) and existing solution NMR structures omit these residues (74,75). Perhaps due to its relative flexibility and high charge density, α-helix 4 allows accommodation of diverse RNA sequences with high affinity. Importantly, the basic residues of α-helix 4 are not well conserved outside of the α-keto receptors (mineralocorticoid receptor, androgen receptor, and progesterone receptor) and may explain differences in RNA-binding across the nuclear receptor family observed previously (20). For example, only two of six arginine and lysine residues are conserved in estrogen receptor, which is reported to not bind to RNA (Supplemental Table S4) (20). Similar low conservation persists across the rest of the family and suggests that the α-keto receptors may exhibit uniquely high affinity RNA-binding among nuclear receptors. This utilization of a basic protein tail to bind RNA is an emerging theme in RNA recognition (76,77).

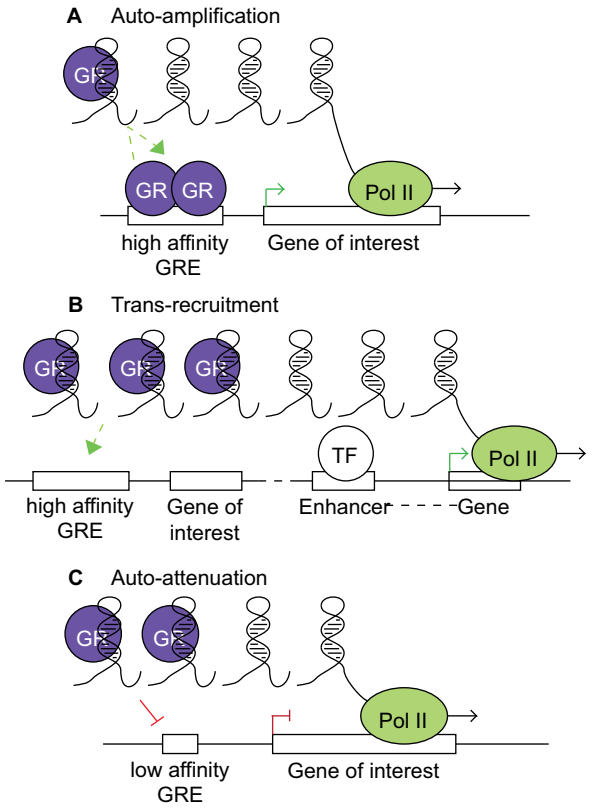

Figure 7. Proposed mechanism for RNA-binding function in vivo. Relative affinities for DNA and RNA *in vivo* may dictate mechanism. (**A**) Accumulation of RNA near a high affinity GRE may serve to maintain a high local concentration of GR for signal amplification. (**B**) TF-activated transcription may accumulate either enhancer RNA or mRNA that serves to recruit GR to sites of active transcription. (**C**) Accumulation of RNA near a low affinity GRE may attenuate DNA-binding, particularly for monomer-bound DNA.

In the cell, the GR-DBD is integral for the function of the receptor where ligand-activated GR alters gene expression through direct DNA-binding to GREs (78,79). Our results suggest that GR RNA-binding activity, which is in the same affinity regime as DNA-binding (15,16), may affect its nuclear function several ways. Recent reports indicate that activated GR is quickly recruited to transcribed enhancers and was separately shown to bind directly to nascent RNA (Figure 7A) (80,81). It is worth considering that favorable protein-protein interactions and general cooperativity between TFs may drive sequence-specific DNA recognition even through a sea of high affinity RNA molecules, for example through previously described interactions between GR and transcription factors AP-1 and NF-kB (1,82,83). After recruitment, active transcription and tethered transcripts may serve as GR binding sites that retain GR at high local concentrations for signal maintenance (Figure 7B). GR is also more quickly exchanged on DNA when compared to other transcription factors, a possible explanation being that RNA competes for binding to disassemble GR from DNA (84–87). In this way, RNA may participate as a transcription-dependent competitor to act as a tunable, self-regulating off switch in the nucleus (Figure 7C). Conversely, RNA-binding may also play a role prior to ligand activation, when GR resides in the cytoplasm as a monomer bound to chaperones proteins (1,88). Delineation of the role of RNA-binding *in vivo* warrants further characterization to test these models, in particular with respect to post-translational modifications (89).

Tight binding between TFs and RNA is emerging as a broad phenomenon with potentially significant biological impact (90). Many TFs have been identified in studies of the RNA-bound proteome, hinting at extensive functional modulations through direct binding (46,91). In depth studies of the RNA-binding activities of several transcription factors, including SMAD3 and NF-κB, show that RNA preference does not correlate to DNA sequence recognition although binding occurs via the same interface, a clear parallel to our findings (35,37,38). Rather, SMAD3 binds with high affinity to RNAs containing large internal loops or bulges and NF-κB binds to distorted RNA helices that structurally mimic DNA (35,37,38). Additional examples include, p53, NF-YA, Sox2, Myc, TFIIIA, and YY1, among others—in all of these cases, it is proposed that RNA-binding modulates genomic DNA-binding *in vivo* (32,33,39–42,66,89,90,92–97).

In summary, we have demonstrated that high affinity RNA-binding by the GR-DBD occurs in a structure-specific rather than sequence-specific mode through a similar, but not identical, binding interface. This implicates broad engagement of GR with RNA partners, providing new avenues for the regulation of TF activity by RNAs.

SUPPLEMENTARY DATA

Supplementary Data are available at NAR Online.

ACKNOWLEDGEMENTS

We would like to thank Jonathan W. Markert and Canessa J. Swanson for their contributions to experimental development in this work and Meagan Y. Nakamoto for contributing control RNAs.

FUNDING

National Institutes of Health [T32GM008732-13 to N.V.P.; R01GM120347 to R.T.B. and D.S.W.]. Funding for open access charge: NIH/University of Colorado, Boulder.
Conflict of interest statement. None declared.

REFERENCES

1. Weikum,E.R., Knuesel,M.T., Ortlund,E.A. and Yamamoto,K.R. (2017) Glucocorticoid receptor control of transcription: precision and plasticity via allostery. *Nat. Rev. Mol. Cell Biol.*, **18**, 159–174.
2. Vockley,C.M., D'Ippolito,A.M., McDowell,I.C., Majoros,W.H., Safi,A., Song,L., Crawford,G.E. and Reddy,T.E. (2016) Direct GR binding sites potentiate clusters of TF binding across the human genome. *Cell*, **166**, 1269–1281.
3. Reddy,T.E., Pauli,F., Sprouse,R.O., Neff,N.F., Newberry,K.M., Garabedian,M.J. and Myers,R.M. (2009) Genomic determination of the glucocorticoid response reveals unexpected mechanisms of gene regulation. *Genome Res*, **19**, 2163–2171.
4. So,A.Y.-L., Cooper,S.B., Feldman,B.J., Manuchehri,M. and Yamamoto,K.R. (2008) Conservation analysis predicts in vivo occupancy of glucocorticoid receptor-binding sequences at glucocorticoid-induced genes. *Proc. Natl. Acad. Sci. U.S.A.*, **105**, 5745–5749.

5. John,S., Sabo,P.J., Thurman,R.E., Sung,M.-H., Biddie,S.C., Johnson,T.A., Hager,G.L. and Stamatoyannopoulos,J.A. (2011) Chromatin accessibility pre-determines glucocorticoid receptor binding patterns. *Nat. Genet.*, **43**, 264–268.
6. Desmet,S.J. and De Bosscher,K. (2017) Glucocorticoid receptors: finding the middle ground. *J. Clin. Invest.*, **127**, 1136–1145.
7. De Bosscher,K., Beck,I.M., Ratman,D., Berghe,W.V. and Libert,C. (2016) Activation of the glucocorticoid receptor in acute inflammation: the SEDIGRAM Concept. *Trends Pharmacol. Sci.*, **37**, 4–16.
8. Kadmiel,M. and Cidlowski,J.A. (2013) Glucocorticoid receptor signaling in health and disease. *Trends Pharmacol. Sci.*, **34**, 518–530.
9. Pufall,M.A. (2015) Glucocorticoids and cancer. *Adv. Exp. Med. Biol.*, **872**, 315–333.
10. Banuelos,J., Shin,S.C. and Lu,N.Z. (2015) A hotspot in the glucocorticoid receptor DNA-binding domain susceptible to loss of function mutation. *Steroids*, **96**, 115–120.
11. Ruiz,M., Lind,U., Gåfvels,M., Eggertsen,G., Carlstedt-Duke,J., Nilsson,L., Holtmann,M., Stierna,P., Wikström,A.C. and Werner,S. (2001) Characterization of two novel mutations in the glucocorticoid receptor gene in patients with primary cortisol resistance. *Clin. Endocrinol. (Oxf.)*, **55**, 363–371.
12. Chandler,V.L., Maler,B.A. and Yamamoto,K.R. (1983) DNA sequences bound specifically by glucocorticoid receptor in vitro render a heterologous promoter hormone responsive in vivo. *Cell*, **33**, 489–499.
13. Luisi,B.F., Xu,W.X., Otwinowski,Z., Freedman,L.P., Yamamoto,K.R. and Sigler,P.B. (1991) Crystallographic analysis of the interaction of the glucocorticoid receptor with DNA. *Nature*, **352**, 497–505.
14. Gewirth,D.T. and Sigler,P.B. (1995) The basis for half-site specificity explored through a non-cognate steroid receptor-DNA complex. *Nat. Struct. Mol. Biol.*, **2**, 386–394.
15. Meijsing,S.H., Pufall,M.A., So,A.Y., Bates,D.L., Chen,L. and Yamamoto,K.R. (2009) DNA binding site sequence directs glucocorticoid receptor structure and activity. *Science*, **324**, 407–410.
16. Hudson,W.H., Youn,C. and Ortlund,E.A. (2013) The structural basis of direct glucocorticoid-mediated transrepression. *Nat. Struct. Mol. Biol.*, **20**, 53–58.
17. Watson,L.C., Kuchenbecker,K.M., Schiller,B.J., Gross,J.D., Pufall,M.A. and Yamamoto,K.R. (2013) The glucocorticoid receptor dimer interface allosterically transmits sequence-specific DNA signals. *Nat. Struct. Mol. Biol.*, **20**, 876–883.
18. Schiller,B.J., Chodankar,R., Watson,L.C., Stallcup,M.R. and Yamamoto,K.R. (2014) Glucocorticoid receptor binds half sites as a monomer and regulates specific target genes. *Genome Biol.*, **15**, 418.
19. Kino,T., Hurt,D.E., Ichijo,T., Nader,N. and Chrousos,G.P. (2010) Noncoding RNA gas5 is a growth arrest- and starvation-associated repressor of the glucocorticoid receptor. *Sci. Signal*, **3**, ra8.
20. Hudson,W.H., Pickard,M.R., de Vera,I.M.S., Kuiper,E.G., Mourtada-Maarabouni,M., Conn,G.L., Kojetin,D.J., Williams,G.T. and Ortlund,E.A. (2014) Conserved sequence-specific lincRNA–steroid receptor interactions drive transcriptional repression and direct cell fate. *Nat.Commun.*, **5**, 5395.
21. Ali,M. and Vedeckis,W.V. (1987) The glucocorticoid receptor protein binds to transfer RNA. *Science*, **235**, 467–470.
22. Park,O.H., Do,E. and Kim,Y.K. (2015) A new function of glucocorticoid receptor: regulation of mRNA stability. *BMB Rep.*, **48**, 367–368.
23. Li,W., Zhai,L., Wang,H., Liu,C., Zhang,J., Chen,W. and Wei,Q. (2016) Downregulation of LncRNA GAS5 causes trastuzumab resistance in breast cancer. *Oncotarget*, **7**, 27778–27786.
24. Mourtada-Maarabouni,M., Hedge,V.L., Kirkham,L., Farzaneh,F. and Williams,G.T. (2008) Growth arrest in human T-cells is controlled by the non-coding RNA growth-arrest-specific transcript 5 (GAS5). *J. Cell Sci.*, **121**, 939–946.
25. Mourtada-Maarabouni,M., Pickard,M.R., Hedge,V.L., Farzaneh,F. and Williams,G.T. (2009) GAS5, a non-protein-coding RNA, controls apoptosis and is downregulated in breast cancer. *Oncogene*, **28**, 195–208.
26. Pickard,M.R. and Williams,G.T. (2015) Molecular and cellular mechanisms of action of tumour suppressor GAS5 LncRNA. *Genes (Basel)*, **6**, 484–499.
27. Pickard,M.R. and Williams,G.T. (2014) Regulation of apoptosis by long non-coding RNA GAS5 in breast cancer cells: implications for chemotherapy. *Breast Cancer Res. Treat.*, **145**, 359–370.
28. Pickard,M.R. and Williams,G.T. (2016) The hormone response element mimic sequence of GAS5 lncRNA is sufficient to induce apoptosis in breast cancer cells. *Oncotarget*, **7**, 10104–10116.
29. Zhang,Y., Su,X., Kong,Z., Fu,F., Zhang,P., Wang,D., Wu,H., Wan,X. and Li,Y. (2017) An androgen reduced transcript of LncRNA GAS5 promoted prostate cancer proliferation. *PLoS One*, **12**, e0182305.
30. Chan,J.A., Krichevsky,A.M. and Kosik,K.S. (2005) MicroRNA-21 Is an antiapoptotic factor in human glioblastoma cells. *Cancer Res.*, **65**, 6029–6033.
31. Zhang,Z., Zhu,Z., Watabe,K., Zhang,X., Bai,C., Xu,M., Wu,F. and Mo,Y.-Y. (2013) Negative regulation of lncRNA GAS5 by miR-21. *Cell Death Differ.*, **20**, 1558–1568.
32. Wai,D.C.C., Shihab,M., Low,J.K.K. and Mackay,J.P. (2016) The zinc fingers of YY1 bind single-stranded RNA with low sequence specificity. *Nucleic Acids Res.*, **44**, 9153–9165.
33. Jeon,Y. and Lee,J.T. (2011) YY1 tethers Xist RNA to the inactive X nucleation center. *Cell*, **146**, 119–133.
34. Davis,B.N., Hilyard,A.C., Nguyen,P.H., Lagna,G. and Hata,A. (2010) Smad proteins bind a conserved rna sequence to promote microrna maturation by drosha. *Mol. Cell*, **39**, 373–384.
35. Dickey,T.H. and Pyle,A.M. (2017) The SMAD3 transcription factor binds complex RNA structures with high affinity. *Nucleic Acids Res.*, **45**, 11980–11988.
36. Rapicavoli,N.A., Qu,K., Zhang,J., Mikhail,M., Laberge,R.-M. and Chang,H.Y. (2013) A mammalian pseudogene lncRNA at the interface of inflammation and anti-inflammatory therapeutics. *eLife*, **2**, e00762.
37. Huang,D.-B., Vu,D., Cassiday,L.A., Zimmerman,J.M., Maher,L.J. and Ghosh,G. (2003) Crystal structure of NF-κB (p50)2 complexed to a high-affinity RNA aptamer. *Proc. Natl. Acad. Sci. U.S.A.*, **100**, 9268–9273.
38. Lebruska,L.L. and Maher,L.J. (1999) Selection and characterization of an RNA Decoy for transcription factor NF-κB. *Biochemistry*, **38**, 3168–3174.
39. Picard,B. and Wegnez,M. (1979) Isolation of a 7S particle from Xenopus laevis oocytes: a 5S RNA-protein complex. *Proc. Natl. Acad. Sci. U.S.A.*, **76**, 241–245.
40. Pelham,H.R. and Brown,D.D. (1980) A specific transcription factor that can bind either the 5S RNA gene or 5S RNA. *Proc. Natl. Acad. Sci. U.S.A.*, **77**, 4170–4174.
41. Setzer,D.R., Menezes,S.R., Del Rio,S., Hung,V.S. and Subramanyan,G. (1996) Functional interactions between the zinc fingers of Xenopus transcription factor IIIA during 5S rRNA binding. *RNA*, **2**, 1254–1269.
42. Cassiday,L.A. and Maher,L.J. III. (2002) Having it both ways: transcription factors that bind DNA and RNA. *Nucleic Acids Res.*, **30**, 4118–4126.
43. Mondragón,E. and Maher,L.J. (2015) RNA aptamer inhibitors of a restriction endonuclease. *Nucleic Acids Res.*, **43**, 7544–7555.
44. Djebali,S., Davis,C.A., Merkel,A., Dobin,A., Lassmann,T., Mortazavi,A.M., Tanzer,A., Lagarde,J., Lin,W., Schlesinger,F. *et al.* (2012) Landscape of transcription in human cells. *Nature*, **489**, 101–108.
45. Iyer,M.K., Niknafs,Y.S., Malik,R., Singhal,U., Sahu,A., Hosono,Y., Barrette,T.R., Prensner,J.R., Evans,J.R., Zhao,S. *et al.* (2015) The landscape of long noncoding RNAs in the human transcriptome. *Nat. Genet.*, **47**, 199–208.
46. Castello,A., Fischer,B., Eichelbaum,K., Horos,R., Beckmann,B.M., Strein,C., Davey,N.E., Humphreys,D.T., Preiss,T., Steinmetz,L.M. *et al.* (2012) Insights into RNA Biology from an atlas of mammalian mRNA-Binding proteins. *Cell*, **149**, 1393–1406.
47. Gasteiger,E., Hoogland,C., Gattiker,A., Duvaud,S., Wilkins,M.R., Appel,R.D. and Bairoch,A. (2005) Protein identification and analysis tools on the ExPASy Server. In: Walker,JM (ed). *The Proteomics Protocols Handbook*. Humana Press, Totowa, NJ, pp. 571–607.
48. Hellman,L.M. and Fried,M.G. (2007) Electrophoretic mobility shift assay (EMSA) for detecting protein-nucleic acid interactions. *Nat. Protoc.*, **2**, 1849–1861.
49. Milligan,J.F., Groebe,D.R., Witherell,G.W. and Uhlenbeck,O.C. (1987) Oligoribonucleotide synthesis using T7 RNA polymerase and synthetic DNA templates. *Nucleic Acids Res.*, **15**, 8783–8798.

50. Nilsen,T.W. (2013) Gel Purification of RNA. *Cold Spring Harb. Protoc.*, **2**, 180–183.
51. Zearfoss,N.R. and Ryder,S.P. (2012) End-labeling oligonucleotides with chemical tags after synthesis. *Methods Mol. Biol.*, **941**, 181–193.
52. Lu,Z., Zhang,Q.C., Lee,B., Flynn,R.A., Smith,M.A., Robinson,J.T., Davidovich,C., Gooding,A.R., Goodrich,K.J., Mattick,J.S. *et al.* (2016) RNA Duplex map in living cells reveals higher-order transcriptome structure. *Cell*, **165**, 1267–1279.
53. Lorenz,R., Bernhart,S.H., Höner zu Siederdissen,C., Tafer,H., Flamm,C., Stadler,P.F. and Hofacker,I.L. (2011) ViennaRNA Package 2.0. *Algorithms Mol. Biol.*, **6**, 26.
54. Rossi,A.M. and Taylor,C.W. (2011) Analysis of protein-ligand interactions by fluorescence polarization. *Nat. Protoc.*, **6**, 365–387.
55. Altschuler,S.E., Lewis,K.A. and Wuttke,D.S. (2013) Practical strategies for the evaluation of high-affinity protein/nucleic acid interactions. *J. Nucleic Acids Investig.*, **4**, 19–28.
56. Privalov,P.L., Dragan,A.I. and Crane-Robinson,C. (2011) Interpreting protein/DNA interactions: distinguishing specific from non-specific and electrostatic from non-electrostatic components. *Nucleic Acids Res.*, **39**, 2483–2491.
57. Manning,G.S. (1969) Limiting laws and counterion condensation in polyelectrolyte solutions I. colligative properties. *J. Chem. Phys.*, **51**, 924–933.
58. Manning,G.S. (2002) Electrostatic free energy of the DNA double helix in counterion condensation theory. *Biophys. Chem.*, **101-102**, 461–473.
59. Williamson,M.P. (2013) Using chemical shift perturbation to characterise ligand binding. *Prog. Nuclear Magn. Reson. Spectrosc.*, **73**, 1–16.
60. Alroy,I. and Freedman,L.P. (1992) DNA binding analysis of glucocorticoid receptor specificity mutants. *Nucleic Acids Res.*, **20**, 1045–1052.
61. Schöne,S., Jurk,M., Helabad,M.B., Dror,I., Lebars,I., Kieffer,B., Imhof,P., Rohs,R., Vingron,M., Thomas-Chollier,M. *et al.* (2016) Sequences flanking the core-binding site modulate glucocorticoid receptor structure and activity. *Nat. Commun.*, **7**, 12621.
62. Smith,C.M. and Steitz,J.A. (1998) Classification of gas5 as a multi-small-nucleolar-RNA (snoRNA) Host gene and a member of the 5′-Terminal oligopyrimidine gene family reveals common features of snoRNA host genes. *Mol. Cell Biol.*, **18**, 6897–6909.
63. Smola,M.J., Christy,T.W., Inoue,K., Nicholson,C.O., Friedersdorf,M., Keene,J.D., Lee,D.M., Calabrese,J.M. and Weeks,K.M. (2016) SHAPE reveals transcript-wide interactions, complex structural domains, and protein interactions across the Xist lncRNA in living cells. *PNAS*, **113**, 10322–10327.
64. Somarowthu,S., Legiewicz,M., Chillón,I., Marcia,M., Liu,F. and Pyle,A.M. (2015) HOTAIR forms an intricate and modular secondary structure. *Mol. Cell*, **58**, 353–361.
65. Pintacuda,G., Wei,G., Roustan,C., Kirmizitas,B.A., Solcan,N., Cerase,A., Castello,A., Mohammed,S., Moindrot,B., Nesterova,T.B. *et al.* (2017) hnRNPK Recruits PCGF3/5-PRC1 to the Xist RNA B-Repeat to establish polycomb-mediated chromosomal silencing. *Mol. Cell*, **68**, 955–969.
66. Ng,S.-Y., Johnson,R. and Stanton,L.W. (2012) Human long non-coding RNAs promote pluripotency and neuronal differentiation by association with chromatin modifiers and transcription factors. *EMBO J.*, **31**, 522–533.
67. Polaski,J.T., Holmstrom,E.D., Nesbitt,D.J. and Batey,R.T. (2016) Mechanistic insights into cofactor-dependent coupling of RNA folding and mRNA transcription/translation by a cobalamin riboswitch. *Cell Rep.*, **15**, 1100–1110.
68. Frank,F., Okafor,C.D. and Ortlund,E.A. (2018) The first crystal structure of a DNA-free nuclear receptor DNA binding domain sheds light on DNA-driven allostery in the glucocorticoid receptor. *Scientific Rep.*, **8**, 13497.
69. Ishmael,F.T., Fang,X., Houser,K.R., Pearce,K., Abdelmohsen,K., Zhan,M., Gorospe,M. and Stellato,C. (2011) The human glucocorticoid receptor as an rna-binding protein: global analysis of glucocorticoid receptor-associated transcripts and identification of a target RNA motif. *J. Immunol.*, **186**, 1189–1198.
70. Battiste,J.L., Mao,H., Rao,N.S., Tan,R., Muhandiram,D.R., Kay,L.E., Frankel,A.D. and Williamson,J.R. (1996) α Helix-RNA major groove recognition in an HIV-1 rev peptide-RRE RNA complex. *Science*, **273**, 1547–1551.
71. Weeks,K.M. and Crothers,D.M. (1991) RNA recognition by Tat-derived peptides: interaction in the major groove? *Cell*, **66**, 577–588.
72. Puglisi,J.D., Chen,L., Blanchard,S. and Frankel,A.D. (1995) Solution structure of a bovine immunodeficiency virus Tat-TAR Peptide-RNA complex. *Science*, **270**, 1200–1203.
73. Cilley,C.D. and Williamson,J.R. (2003) Structural mimicry in the phage φ21 N peptide–boxB RNA complex. *RNA*, **9**, 663–676.
74. van Tilborg,M., Bonvin,A.M., Hård,K., Davis,A.L., Maler,B., Boelens,R., Yamamoto,K.R. and Kaptein,R. (1995) Structure refinement of the glucocorticoid receptor-DNA binding domain from NMR data by relaxation matrix calculations. *J. Mol. Biol.*, **247**, 689–700.
75. Baumann,H., Paulsen,K., Kovacs,H., Berglund,H., Wright,A.P.H., Gustafsson,J.A. and Haerd,T. (1993) Refined solution structure of the glucocorticoid receptor DNA-binding domain. *Biochemistry*, **32**, 13463–13471.
76. Järvelin,A.I., Noerenberg,M., Davis,I. and Castello,A. (2016) The new (dis)order in RNA regulation. *Cell Commun. Signal.*, **14**, 9.
77. Ozdilek,B.A., Thompson,V.F., Ahmed,N.S., White,C.I., Batey,R.T. and Schwartz,J.C. (2017) Intrinsically disordered RGG/RG domains mediate degenerate specificity in RNA binding. *Nucleic Acids Res.*, **45**, 7984–7996.
78. Nagy,L. and Schwabe,J.W.R. (2004) Mechanism of the nuclear receptor molecular switch. *Trends Biochem. Sci.*, **29**, 317–324.
79. Strahle,U., Klock,G. and Schutz,G. (1987) A DNA sequence of 15 base pairs is sufficient to mediate both glucocorticoid and progesterone induction of gene expression. *Proc. Natl. Acad. Sci. U.S.A.*, **84**, 7871–7875.
80. McDowell,I.C., Barrera,A., D'Ippolito,A.M., Vockley,C.M., Hong,L.K., Leichter,S.M., Bartelt,L.C., Majoros,W.H., Song,L., Safi,A. *et al.* (2018) Glucocorticoid receptor recruits to enhancers and drives activation by motif-directed binding. *Genome Res.*, **28**, 1272–1284.
81. Bao,X., Guo,X., Yin,M., Tariq,M., Lai,Y., Kanwal,S., Zhou,J., Li,N., Lv,Y., Pulido-Quetglas,C. *et al.* (2018) Capturing the interactome of newly transcribed RNA. *Nat. Methods*, **15**, 213–220.
82. Miner,J.N. and Yamamoto,K.R. (1992) The basic region of AP-1 specifies glucocorticoid receptor activity at a composite response element. *Genes Dev.*, **6**, 2491–2501.
83. De Bosscher,K., Vanden Berghe,W. and Haegeman,G. (2003) The interplay between the glucocorticoid receptor and nuclear factor-κb or activator protein-1: molecular mechanisms for gene repression. *Endocr. Rev.*, **24**, 488–522.
84. McNally,J.G., Müller,W.G., Walker,D., Wolford,R. and Hager,G.L. (2000) The glucocorticoid receptor: rapid exchange with regulatory sites in living cells. *Science*, **287**, 1262–1265.
85. Becker,M., Baumann,C., John,S., Walker,D.A., Vigneron,M., McNally,J.G. and Hager,G.L. (2002) Dynamic behavior of transcription factors on a natural promoter in living cells. *EMBO Rep.*, **3**, 1188–1194.
86. Stavreva,D.A., Müller,W.G., Hager,G.L., Smith,C.L. and McNally,J.G. (2004) Rapid glucocorticoid receptor exchange at a promoter is coupled to transcription and regulated by chaperones and proteasomes. *Mol. Cell Biol.*, **24**, 2682–2697.
87. Meijsing,S.H., Elbi,C., Luecke,H.F., Hager,G.L. and Yamamoto,K.R. (2007) The ligand binding domain controls glucocorticoid receptor dynamics independent of ligand release. *Mol. Cell Biol.*, **27**, 2442–2451.
88. Picard,D., Khursheed,B., Garabedian,M.J., Fortin,M.G., Lindquist,S. and Yamamoto,K.R. (1990) Reduced levels of hsp90 compromise steroid receptor action in vivo. *Nature*, **348**, 166–168.
89. Riley,K.J.-L. and Maher,L.J. (2007) p53–RNA interactions: new clues in an old mystery. *RNA*, **13**, 1825–1833.
90. Long,Y., Wang,X., Youmans,D.T. and Cech,T.R. (2017) How do lncRNAs regulate transcription? *Sci. Adv.*, **3**, eaao2110.
91. Baltz,A.G., Munschauer,M., Schwanhäusser,B., Vasile,A., Murakawa,Y., Schueler,M., Youngs,N., Penfold-Brown,D., Drew,K., Milek,M. *et al.* (2012) The mRNA-Bound proteome and its global occupancy profile on protein-coding transcripts. *Mol. Cell*, **46**, 674–690.
92. Hung,T., Wang,Y., Lin,M.F., Koegel,A.K., Kotake,Y., Grant,G.D., Horlings,H.M., Shah,N., Umbricht,C., Wang,P. *et al.* (2011)

Extensive and coordinated transcription of noncoding RNAs within cell cycle promoters. *Nat. Genet.*, **43**, 621–629.
93. Ng,S.-Y., Bogu,G.K., Soh,B.S. and Stanton,L.W. (2013) The long noncoding RNA RMST interacts with SOX2 to regulate neurogenesis. *Mol. Cell*, **51**, 349–359.
94. Tseng,Y.-Y., Moriarity,B.S., Gong,W., Akiyama,R., Tiwari,A., Kawakami,H., Ronning,P., Reuland,B., Guenther,K., Beadnell,T.C. *et al.* (2014) PVT1 dependence in cancer with MYC copy-number increase. *Nature*, **512**, 82–86.
95. Engelke,D.R., Ng,S.-Y., Shastry,B.S. and Roeder,R.G. (1980) Specific interaction of a purified transcription factor with an internal control region of 5S RNA genes. *Cell*, **19**, 717–728.
96. Sigova,A.A., Abraham,B.J., Ji,X., Molinie,B., Hannett,N.M., Eric Guo,Y., Jangi,M., Giallourakis,C.C., Sharp,P.A. and Young,R.A. (2015) Transcription factor trapping by RNA in gene regulatory elements. *Science*, **350**, 978–981.
97. Zhou,L., Sun,K., Zhao,Y., Zhang,S., Wang,X., Li,Y., Lu,L., Chen,X., Chen,F., Bao,X. *et al.* (2015) Linc-YY1 promotes myogenic differentiation and muscle regeneration through an interaction with the transcription factor YY1. *Nat. Commun.*, **6**, 10026.
98. Dragan,A.I., Read,C.M., Makeyeva,E.N., Milgotina,E.I., Churchill,M.E.A., Crane-Robinson,C. and Privalov,P.L. (2004) DNA Binding and Bending by HMG Boxes: Energetic Determinants of Specificity. *J. Mol. Biol.*, **343**, 371–393.
99. Zuker,M. (2003) Mfold web server for nucleic acid folding and hybridization prediction. *Nucleic Acids Res.*, **31**, 3406–3415.